The Influence of Microstructure on the Tensile and Fatigue Behavior of SAE 6150 Steel

T. Alp and A. Wazzan

(Submitted 6 July 2000)

The tensile and reverse-bending fatigue behaviors of the SAE 6150 steel in the dual-phase (DP), fully martensitic, and tempered states, respectively, have been investigated using mechanical tests, scanning electron microscopy (SEM), energy-dispersive x-ray (EDX) microscopy, and optical microscopy. Residual stresses, inherent microcracks, and retained austenite films in the martensitic steel, quenched from 900 °C, lead to the development of inferior tensile and fatigue strength. Tempering at 700 °C relieves the residual stresses associated with martensite, causes the precipitation of microalloy carbides (MACs), and thus results in superior strength, increased fatigue resistance, and moderate ductility. The DP microstructure, consisting of martensite islets in a ferrite matrix, gives rise to a combination of good strength, excellent ductility, and commendable fatigue characteristics. MAC in the tempered steel and martensite islands in the DP variant enhance fatigue performance by causing crack tip deflection and concomitant crack path tortuosity. Strain incompatibility between martensite and ferrite in the DP steel, and cementite films and ferrite in the tempered variant are identified as fatigue crack initiation sites.

Keywords dual-phase steels, fatigue behavior, SAE 6150 steel, tensile behavior

1. Introduction

The high-strength low-alloy (HSLA) steels known as dual-phase (DP) steels were developed to improve safety standards and fuel economy. The microstructure of these steels essentially consists of a fine-grained ferritic matrix and a uniform dispersion of hard martensite islands.[1-5] This microstructure may be obtained by controlled rolling from the fully austenitized state or by intercritically annealing the steel in the (α + γ) region of the equilibrium phase diagram[6] to allow phase equilibration. Subsequent quenching permits a fraction of the austenite to be converted to epitaxial ferrite, and the remainder to martensite. Depending on the steel chemistry and processing parameters, intermediate transformation products, lower bainite and pearlite may form, and some untransformed austenite may be retained in amounts varying from 2-9 vol.%.[6-9] Retained austenite occurs in the form of interlath films[9] or as fine particles that are too small to undergo the martensite transformation.[10] Low cooling rates and high intercritical annealing temperatures (ICTs) favor austenite retension.[7,11] Retained austenite enhances steel ductility, and upon plastic deformation it transforms to martensite, thereby increasing the tensile strength of steel.[12]

To transform austenite to martensite, quenching from the ICT must be sufficiently rapid or the austenite must have appropriate martensite hardenability. Severe quenching is objectionable due to consequential residual stresses, associated distortions, and property variations. The martensitic hardenability of austenite has been shown to vary with the chemistry[10,13] and dispersion[14,15] of austenite during cooling. Thus, microalloying additions of V, Mo, and Cr in a C-Mn base steel exercise a paramount influence in determining the martensitic hardenability of austenite.[16,17] Although the amount of austenite is greater at higher ICTs, a smaller fraction of it may transform to martensite due to its lower hardenability, which is caused partly by decreasing the C content of austenite with increasing ICTs. However, during cooling, expitaxial ferrite growth into austenite may occur until the C enrichment of austenite attains the required level to transform the remaining austenite into a mixture of ferrite, carbide, or martensite.

Hansen and Bramfitt[16] have indicated that intercritical annealing at low temperature (740 °C) for 1 h followed by slow cooling gives rise to manganese (Mn) enrichment of the austenite and increases its hardenability near the austenite/ferrite interface, resulting in the formation of a martensite rim around the austenite particle, the center of which transforms to a ferrite/carbide aggregate at higher temperatures. Thus, the amount of austenite that forms and its chemical composition during intercritical annealing are determined, for short amounts of time and low temperatures, by a paraequilibrium in which C alone is partitioned between ferrite and austenite or by a full equilibrium that requires high annealing temperatures and prolonged annealing times when substitutional solute atoms also partition between the phases.

DP steels are known to have high ambient-temperature fatigue threshold values[18-24] ascribed to higher crack closure levels resulting from a combination of mode I (tensile) and mode II (shear) crack growth.[19] High crack closure levels in DP steels have been attributed to the highly tortuous nature of the crack propagation path in ferrite and to crack deflection at the interphase boundaries, particularly at ferrite/martensite interfaces.

Research in the last two decades has focused on C-Mn DP steels with low-C (C < 0.2%) in order to enhance both form-

T. Alp and **A. Wazzan,** King Abdulaziz University, Faculty of Engineering, Chemical & Materials Engineering Department, P.O. Box 80204, Jeddah 21589, Saudi Arabia. Contact e-mail: tyalp1@hotmail.com.

Table 1 Chemical Composition of SAE 6150 Steel

C	Mn	Si	S	P	Mo	Cu	Sn	Al	Cr	Ni	V	Fe
0.51	0.82	0.24	<0.002	<0.005	0.06	0.18	0.013	0.035	1.04	0.2	0.17	balance

ability and strength for weight saving in flat products. The effect of intercritical treatment on medium-C steels has not been duly investigated. Although cold formability may not be a prime concern in massive, load-bearing engineering components, strength improvements and concomittant weight savings may still warrant DP microstructures in thick sections that are manufactured from medium-C steels. This article discusses the influence of intercritical annealing followed by quenching on the mechanical behavior of the SAE 6150 steel under static tension and alternating stress conditions, and compares the microstructure and properties of the DP steel with those of the fully martensitic and tempered variants.

2. Experimental Procedures

The chemical composition of the SAE 6150 steel is given in Table 1. The steel, which was processed at Brinsworth Strip Mills, Rotherham, England, was supplied in the form of a hot-rolled, cold-finished 3 mm thick plate. The steel, as received, contained ferrite and pearlite, with a certain amount of MAC precipitates.

Tensile and fatigue test specimens of the geometrical configuration indicated in Fig. 1 were machined such that the flat surfaces of the specimens were parallel to the rolling plane, and the longitudinal axis of the specimens lay parallel to the rolling direction. The thermal treatments that were applied in order to produce different microstructures fell into three categories.

1. Intercritical annealing of the steel at 740 °C for 30 min in the ($\alpha + \gamma$) phase field of the Fe-C equilibrium phase diagram followed by quenching into iced brine at −10 °C was carried out to produce a DP microstructure consisting of martensite islands in a ferrite matrix.
2. Full austenitization at 900 °C for 30 min followed by quenching into iced brine at −5 °C to obtain a fully martensitic microstructure.
3. Tempering of the steel at 700 °C for 30 min to decompose the martensite produced by the treatment in category 2 and to obtain a dispersion of carbide particles embedded in a ferrite matrix. The tempered specimens were quenched into an oil bath held at room temperature to avoid the segregation of nonmetallic impurities to grain boundaries and associated loss of toughness, which may result from slow cooling rates.

All specimens were annealed in argon atmosphere.

The cooling rates reported for parts 1, 2, and 3 are the averaged values measured over the first half of the temperature decrease. A cooling curve for each specimen was obtained using a chromel/alumel thermocouple spot welded to the center of the flat surface of the specimen shoulder.

Metallographic specimens were sectioned from the midportion of heat-treated fatigue specimens. Quantitative analysis of microstructural constituents was carried out by point counting on selectively etched phases. The etching of flat surfaces was performed in 2% solutions of either nital or picral.

All specimens were finely polished to 0.25 μm finish and fatigue tested in reverse-bending mode. The alternating stress was varied in the range $0 - \sigma$, where $\sigma < \sigma_y$.

Conventional scanning electron microscopy (SEM), and energy-dispersive x-ray (EDX) techniques were employed to study the salient features of both etched flat surfaces and unetched fracture surfaces, respectively.

3. Discussion of Results

3.1 The Microstructure of DP Steel

The microstructure and the resulting mechanical properties of the DP steel primarily depend upon the volume fraction of the austenite at the ICT (740 °C), the specific effects of the alloying additions, which in turn determine the martensite hardenability, and the rate of cooling from the ($\gamma + \alpha$) phase field. At the very rapid quenching rate adopted (755 Ks^{-1}), virtually all of the austenite present at the ICT is transformed to martensite, with no new ferrite forming during cooling before the temperature decreases to the martensite start temperature (Ms) of the austenite. However, as observed by Thomas et al.[25] a certain amount of interlath austenite, usually in the form of thin films, is encountered.

The influence of alloying additions on the nature and volume fraction of the transformation products that form upon cooling the steel from the ICT is of great significance in determining the final mechanical properties. Both chromium (Cr) and vanadium (V), at the appropriate temperature and in sufficiently high concentrations, form their respective carbides, which are thermodynamically more stable in austenite than in cementite. The solubility product data[26,27] imply that at 740 °C all the V in the steel used in the present investigation would be dissolved in austenite. Considering that Cr has a higher solubility in austenite than V, no Cr carbide precipitation is anticipated at 740 °C.

V and Cr have a similar effect on the Fe-C equilibrium phase diagram. They raise the Ae_3 phase boundary and give rise to eutectoid shifts to lower carbon contents. Figure 2 shows the influence of Cr on the γ phase field in Fe-C alloys.[28] Accordingly, at a given ICT, Cr and V decrease the volume fraction of austenite and increase its carbon (C) content.

In practical terms, the hardenability of a steel quenched to contain martensite is determined by its martensite content. The quantity of martensite produced by quenching a steel at a constant rate from a given ICT is controlled by the amount of austenite and its martensitic hardenability. The latter is essentially defined in terms of the volume fraction of austenite that

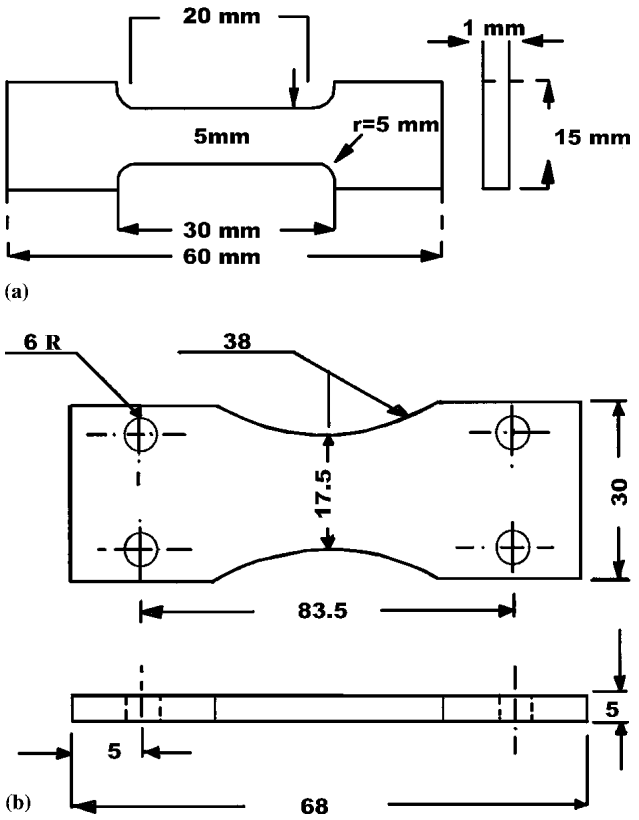

Fig. 1 (**a**) Configuration of tensile test specimen. (**b**) Configuration of fatigue test specimen

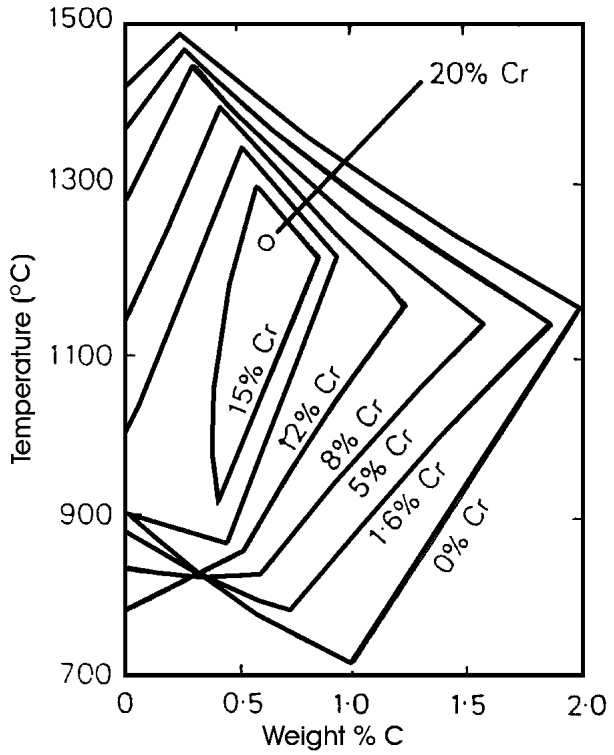

Fig. 2 The effect of Cr on the γ-phase field

is converted to martensite and the way the cooling rate influences that fraction.

Under equilibrium conditions at 740 °C, a plain carbon steel containing 0.5% C is estimated to have 73% austenite. The C concentration of this austenite is 0.68%. However, the experimentally determined values of austenite content are found to be closer to the paraequilibrium values than to the equilibrium values[6,10] for a short intercritical annealing time (30 min) and a low ICT (740 °C). Thus, less than the theoretically computed fraction of austenite would be present at the ICT. Shen and Priestner[13] determined, as a function of the wt.% of C in austenite, the percentage of austenite that is transformed to martensite in low-carbon boron steels, using different cooling rates. Their data indicate that, on brine quenching, virtually all austenite transforms to martensite, irrespective of the C content of the austenite. The extrapolation of their data shows that both water-quenching and oil-quenching cause 100% of the austenite to transform to martensite for an austenite C content of approximately 0.3%. It appears, therefore, that at lower cooling rates than oil-quenching and for C contents of austenite lower than 0.3%, less than 100% of the austenite of their partially austentized steel at 800 °C transformed to martensite.

Therefore, in the present investigation, the C enrichment of austenite at 740 °C arising from the elevation of Ae_3 phase boundary due to the presence of Cr and V, in addition to the effect of every rapid cooling rate from 740 °C, causes maximum hardenability. The cooling curves obtained upon quenching from the (α + γ) phase field at 740 °C, and γ-phase field at 900 °C, respectively, are superimposed on the isothermal transformation diagram of the SAE 6150 steel[29] shown in Fig. 3. Accordingly, the transformation products obtained on quenching from 740 °C primarily consist of old ferrite and martensite. Figure 4 illustrates martensite islands in an evidently deformed ferrite matrix in the vicinity of the necked region of a tensile test specimen.

3.2 The Microstructure of Quenched and Tempered Steel

Quenching plain carbon and low-alloy steels containing up to 0.5% carbon from the austenite phase region results in martensite with lath-like or plate-like morphology. The volume fraction of martensite, f, formed on quenching to any temperature T_q may be estimated by the following equation:

$$f = 1 - \exp - [0.011(M_s - T_q)] \quad \text{(Eq 1)}$$

which predicts the amount of martensite to be only a function of the degree of undercooling below M_s.[29] The M_s temperature is decreased significantly with the increasing percentage of C,[30] and to a lesser extent by Cr, Mn, and certain other alloying elements.[31] Accordingly, a low M_s temperature engenders a reduced volume fraction of martensite. Hence, a substantial volume fraction of retained austenite may result in quenched medium- and high-carbon steels. The findings of Speich[32] indicate that a 0.5% C steel may contain about 5% (by volume) of the retained austenite.

The M_s temperature of the SAE 6150 steel shown in Fig. 3 is 292 °C. This perfectly tallies with the M_s value of 291.7 °C that we calculated using Andrews' empirical relationship, as

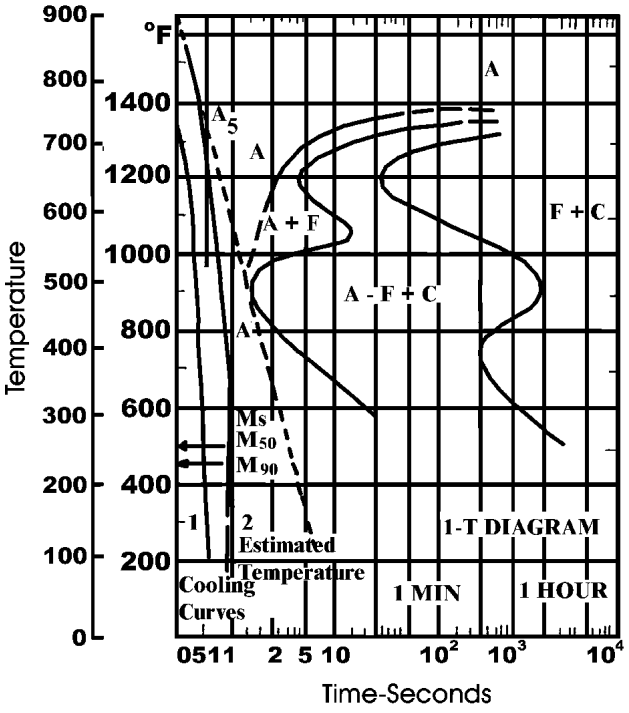

Fig. 3 Isothermal transformation diagram of the SAE 6150 steel with superimposed cooling curves for quenching from 740 °C (1) and 900 °C (2) as arrowed.

quoted by Honeycombe.[26] Substituting this value for the M_s temperature in Eq 1 yields a martensite volume fraction of about 0.96. The balance of the approximately 4% volume fraction is thought to correspond to the amount of retained austenite. This is in good agreement with the amount of retained austenite that was determined experimentally by Speich.[32]

The structure of martensite has been shown to contain a high density of tangled dislocations that are capable of storing considerable strain energy, and thin films of retained austenite.[25-33] Furthermore, the impingement of martensitic crystalites during the evolution of the martensite microstructure gives rise to the development of localized strains that are sufficiently large to cause microcracks to form in the martensite phase.[34] Indeed, as martensite grows at extremely rapid rates of the order of 10^{-7} s, and being accompanied by a substantial volume increase, the dynamic stresses internally generated under these conditions also could cause the nucleation of the microvoids that are occasionally detected on specimen surfaces. As a consequence of these distinctive features cited above, martensite decomposes into cementite and ferrite when tempered at a sufficiently high temperature below Ac_1. Tempering the SAE 6150 steel at 700 °C causes the precipitation of the carbides of VC, Cr_7C_3, and Mo_2C in addition to cementite. Minute platelets of fcc VC, precipitate heterogenously on the dislocations within the ferrite grains and give rise to substantial strengthening. VC is more stable than Cr_7C_3 and Mo_2C, and persists in the form of a fine dispersion even after prolonged exposures at 700 °C. However, extended tempering at 700 °C causes the VC plates to coarsen and eventually to spheroidize. At this temperature, the carbide Cr_7C_3 coarsens much more rapidly than VC and contributes less significantly to the hardening process.

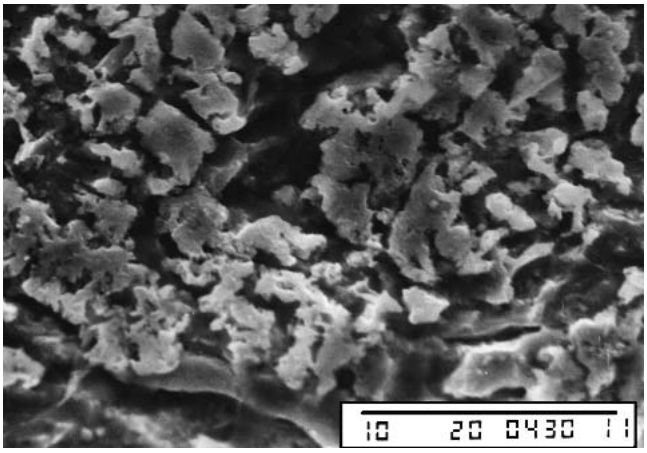

Fig. 4 SEM view of a flat surface close to the necked region showing martensite islands in a ferrite matrix (nital etching)

Table 2 Mechanical Properties of the SAE 6150 Steel (a)

Processing Conditions	σ_y	UTS	σ_b	el, %	RA, %	BHN
		MPa				
AR	…	758	500	12.9	53.8	66
DP	459	590	342	25.0	69.0	56
M	…	…	146	1.9	1.5	90
T	757	819	594	15.4	40.7	68

(a) AR: as received; DP: dual-phase steel with small amount of pearlite; M: martensitic; T: tempered; σ_y: yield stress; σ_b: breaking stress; BHN: Brinell hardness; UTS: ultimate tensile strength; el: elongation; RA: reduction in area.

3.3 Tensile Properties of SAE 6150 Steel

The mechanical properties of the SAE 6150 steel processed under different conditions are listed in Table 2. The DP steel specimens exhibit the highest tensile ductility and reduction in area. The combination of excellent ductility and high strength is attributed to the presence of a highly ductile ferrite matrix and to hard martensite islands, respectively (Fig. 4).

The stress-strain curve of the DP steel shows a distinct yield point that usually is not observed in low-C microalloy DP steels (Fig. 5). The occurrence of a yield point in these steels has been attributed to the presence of pearlite. Figure 6 shows a small pearlite patch that occasionally is encountered in the DP steel.

Specimens containing predominantly plate martensite (Fig. 7) are characterized by high hardness, low strength, and negligible plasticity. The residual stresses induced by martensite transformation are thought to be responsible for the premature failure of this steel under tensile loading. SEM observations of the fracture surface show a typically intergranular mode of fracture (Fig. 8 right) with plastic deformation of the retained austenite (Fig. 8 left).

The tempered steel exhibits exceptionally high strength and moderate tensile ductility. Tempering at 700 °C rapidly decom-

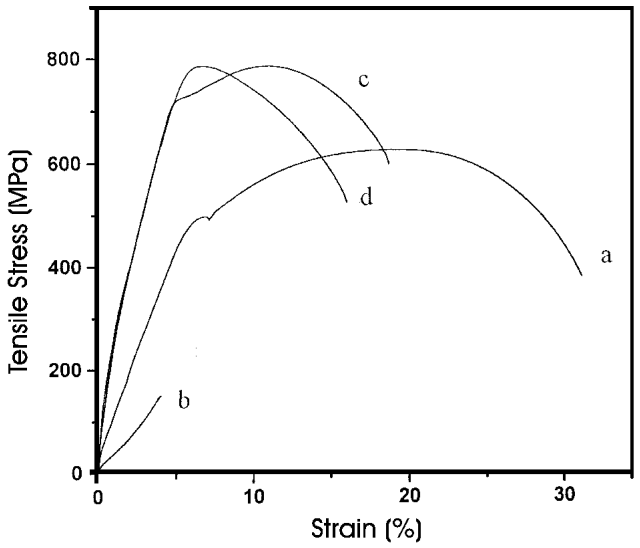

Fig. 5 Stress-strain curves of the SAE 6150 steel processed to contain **(a)** DP, **(b)** martensite, **(c)** tempered microstructure, and **(d)** as received

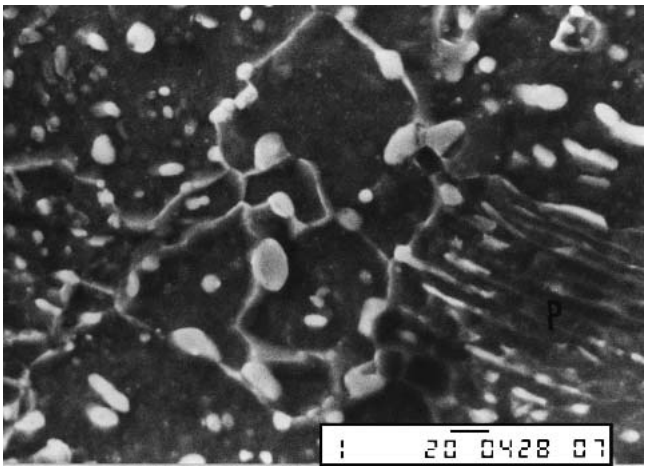

Fig. 6 A small pearlite patch (labeled P in the lower right corner) in the DP microstructure (picral etch)

poses martensite and anneals out the residual stresses associated with it. This results in a great improvement in ductility and strength. However, the most significant contribution to strength arises from the precipitation of the microalloy carbides VC, Mo_2C, and Cr_7C_3. Figure 9 illustrates the fine intragrain dispersion of VC and the rod-like particles of Mo_2C that are heterogeneously precipitated on the dislocations within ferrite grains, together with Cr_7C_3 particles, which have a relatively coarser grain-boundary. The tensile fracture surfaces of tempered specimens reveal extensive dimpling, which is indicative of ductility (Fig. 10).

3.4 Fatigue Properties of SAE 6150 Steel

3.4.1 The DP Steel. Figure 11 illustrates the S-N curves of the SAE 6150 steel in three differently processed conditions.

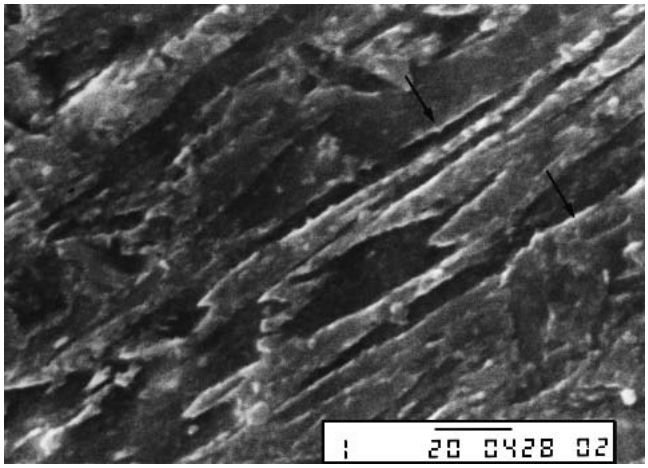

Fig. 7 Massive martensite plates with thin films of retained austenite in between (arrowed) nital etching

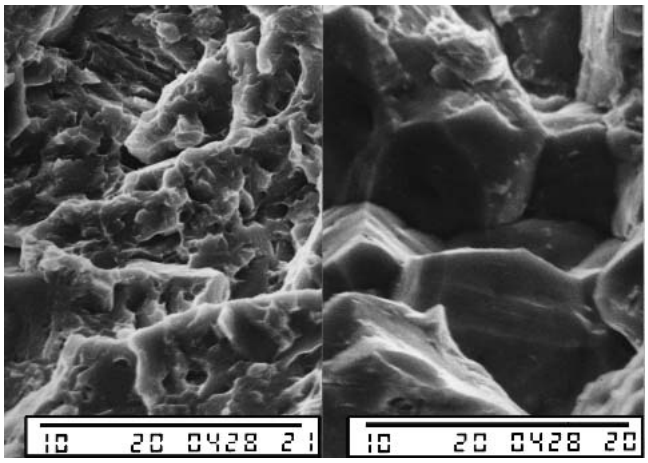

Fig. 8 (**Right**) intergranular fracture and (**left**) plastically deformed retained austenite in a predominantly martensitic steel

The DP steel is characterized by the absence of a clearly defined endurance limit. The fatigue limit exhibited by the DP steel at 10^7 cycles (110 MPa) is measurably lower than the endurance limits of the martensitic (190 MPa), and tempered (240 MPa) variants, respectively. One of the most important factors that is suspected to influence the fatigue resistance of the DP steel appears to be the residual stresses that are induced by martensite transformation. Martensite transformation is accompanied by a volume increase of 2-4%,[35,36] which generates compressive stresses in the martensite islands while the ferrite matrix around them is stressed in tension. Clearly, residual tensile stresses, which are computed to have a maximum value of the order of the yield strength of the ferrite and to decay exponentially from the martensite/ferrite interface,[37] are additive to the applied tensile stress.

The strain incompatibility induced by residual stresses between the hard martensite phase and the ductile ferrite matrix prompts fatigue crack initiation along the martensite/ferrite interfaces. The ensuing crack propagation, which is assisted by

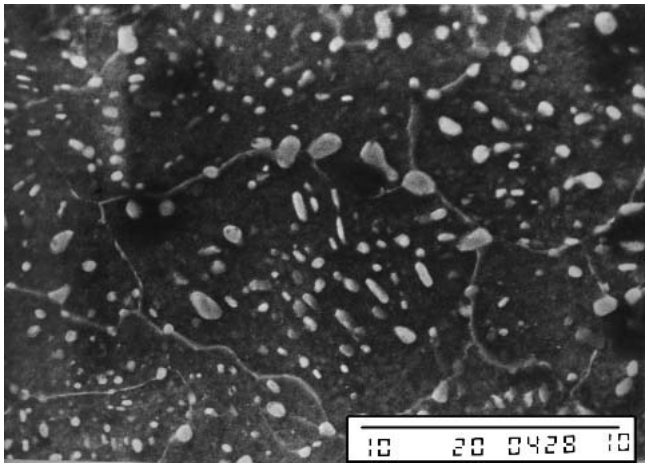

Fig. 9 Fine intragrain VC dispersion, rod-shaped Mo_2C particles, and grain boundary Cr_7C_3 in tempered steel (nital etching)

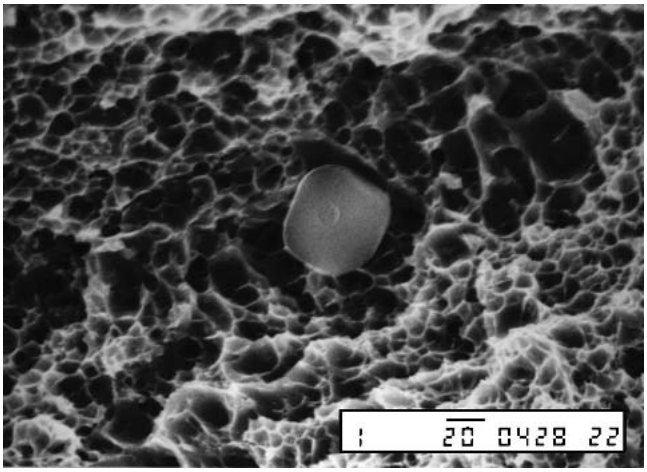

Fig. 10 VC precipitate against the background of a microdimpled matrix in the fracture surface of tempered steel

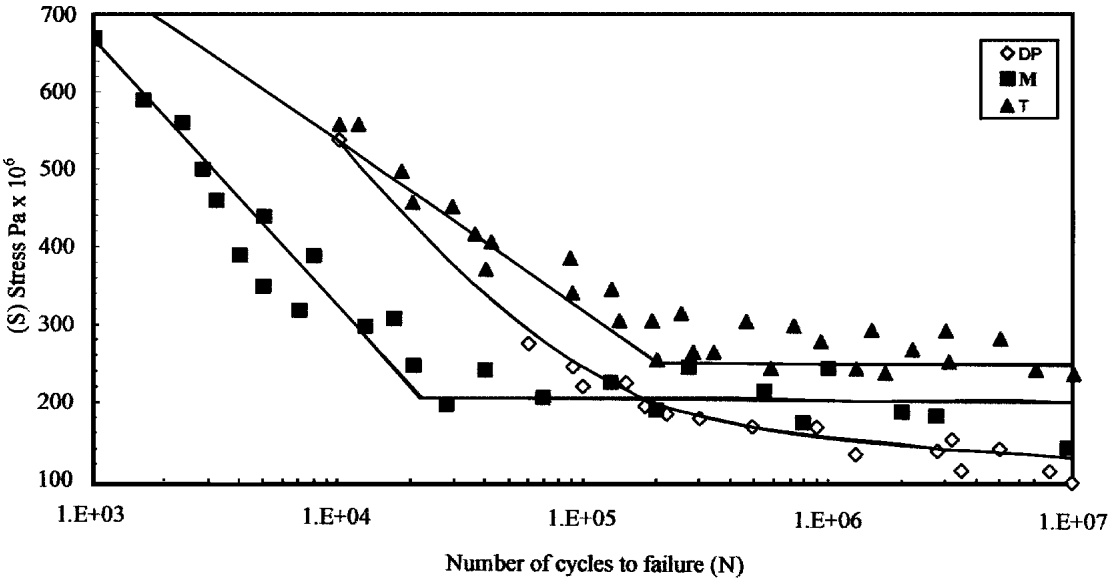

Fig. 11 S-N curves of SAE 6510 steel with tempered (T), DP, and martensite (M) microstructures

the residual tensile stresses in the matrix, takes place preferentially through the ductile ferrite phase. Figure 12 depicts typical embryonic microcracks that are nucleated in ferrite in the early stages of fatigue life. The ferrite phase connectivity in the DP microstructure has an important effect on the mechanical behavior of the steel. A continuous ferrite network results in lower strengths and threshold stress intensities by concentrating the plastic deformation in the ferrite at the crack tip. However, the ductile matrix at the crack tip tends to accommodate the stress by crack tip blunting, which in turn retards crack growth kinetics until the matrix of the crack tip work hardens as a result of repeated strain cycles. Higher stress levels would cause a greater amount of work hardening and would hasten fatigue failure. Suzuki and McEvily[18] have shown that the inversion of the phase morphology from a continuous ferrite to a continuous martensite network gives rise to increased strength and to increased fatigue crack extension resistance. The present study confirmed a previous observation that in a continuous ferrite microstructure individual martensite islands do not shield the crack tip as effectively as a continuous martensite network would. The shielding effect is limited to crack tip deflections alone.[22]

The fracture surface of fatigued DP steel specimens is characterized by discontinuous striation marks (Fig. 13a). Discontinuities in striations are thought to be related to the presence of hard martensite islands. The numerous secondary microcracks observed in Fig. 13(b) are believed to have nucleated at martensite/ferrite interfaces in locations of maximum residual stresses. The stair-like profile of these microcracks, which often are encountered, suggests that a crack-tip deflection mechanism was operative. Also, pearlite patches, which are occasionally encountered in DP steel specimens, are thought to influence the fatigue process negatively. Pearlite has been shown to possess inferior fatigue resistance compared to mar-

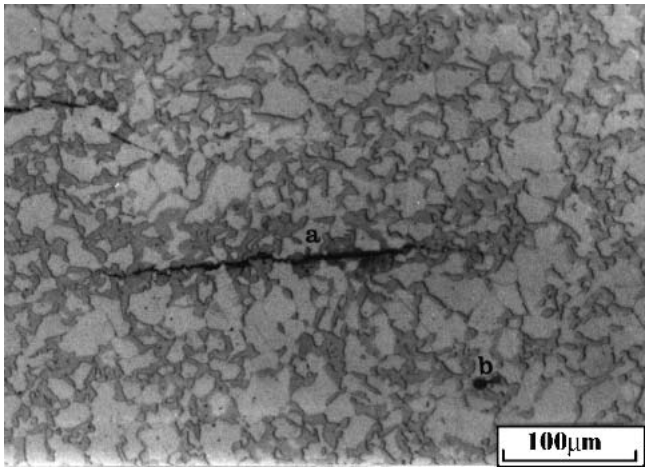

Fig. 12 Crack initiation sites in DP SAE 6150 steel **(a)** at the martensite/ferrite interface and **(b)** at a microvoid. Crack growth is in the ferrite matrix (picral etching, optical micrograph, magnification 300×).

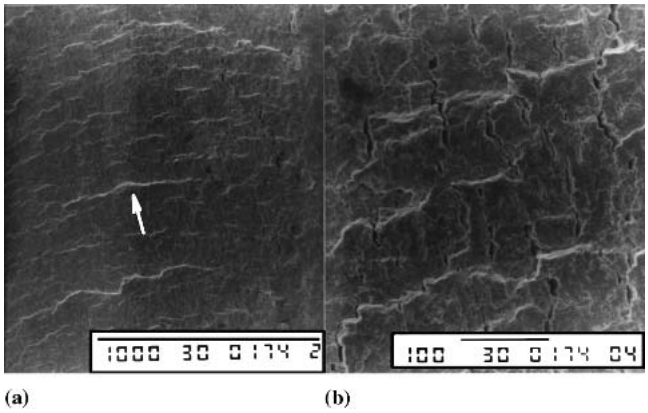

Fig. 13 (**a**) SEM exhibiting discontinuous striation marks in the DP SAE 6150 steel. Arrow indicates direction of macroscopic crack propagation. (**b**) Secondary microcracks at martensite/ferrite interfaces exhibiting a stair-like profile

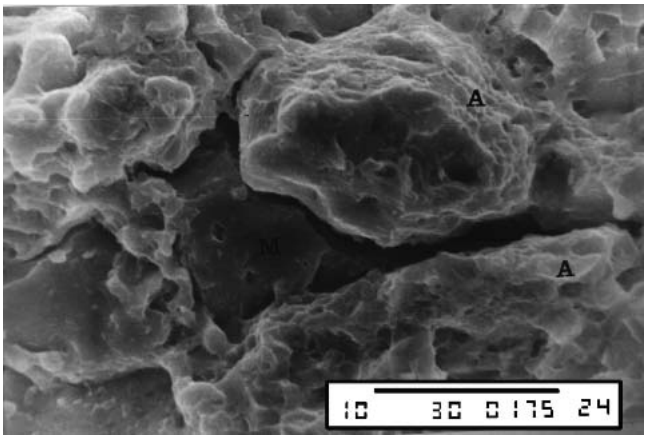

Fig. 14 Microdimples in the austenite film (A) between martensite grains (M) and secondary cracks at austenite/martensite interfaces

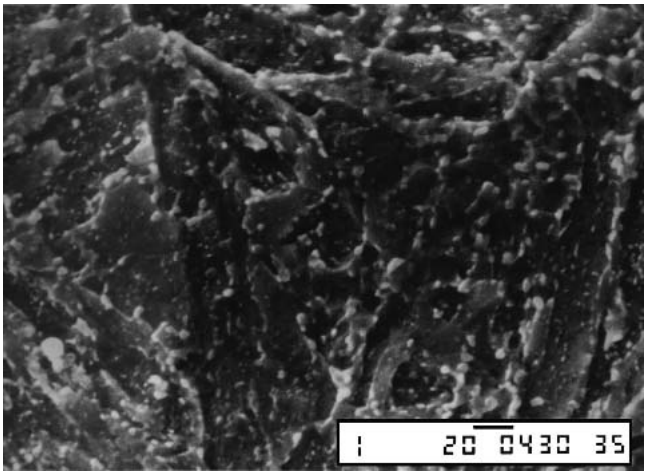

Fig. 15 Fine dispersion of VC precipitates within ferrite in tempered steel. The traces of previous martensite plates are still recognizable (nital etching).

tensite.[38] Ferrite/cementite interfaces are likely to constitute additional potential crack initiation sites.

3.4.2 The Martensitic Steel. The microstructure obtained upon quenching from 900 °C is predominantly martensitic, with some austenite films occurring at prior austenite grain boundaries. The strength level of martensite attained is determined largely by its C content[39] and detailed structure. The fatigue limit of several medium-C alloy steels (i.e., SAE 1340, 4042, 4340, 5140, and 80B40) has been shown to increase with increasing amount of martensite.[40] The massive martensite plates dominating the microstructure in the steel increase the fatigue life by providing effective shielding of the crack tip. Nonetheless, the microcracks are inherently present in martensite plates[34] and the microvoids nucleated in the wake of martensite transformation facilitate crack initiation and thereby shorten the fatigue life of this steel. The S-N curves of the DP and martensite steels intersect at a stress level of approximately 200 MPa when both steels endure about 2×10^5 cycles to failure. Above this stress level, the DP steel exhibits a clearly superior fatigue resistance compared to the martensitic variant.

SEM observations of fatigued specimens with martensite microstructures manifest predominantly brittle intergranular modes of fracture (Fig. 14). Retained austenite films that are usually observed on martensite facets appear to be deformed. This is evidenced by the minute dimples observed in the regions labeled (A). The strain incompatibility between retained austenite and martensite renders the austenite/martensite interface as another favorable location for crack nucleation.

3.4.3 The Tempered Steel. Tempering at 700 °C decomposes martensite and thus relieves the residual stresses associated with it. Hence, the crack initiation stage is prolonged due to the elimination of martensite/austenite interfaces, which, as explained earlier, act as crack nucleation sites. Furthermore, tempering brings about significant MAC precipitation. Vanadium, being a strong carbide former, precipitates in the form of fine dispersion of VC platelets on dislocations within the ferrite grains and gives rise to a marked strengthening effect. VC

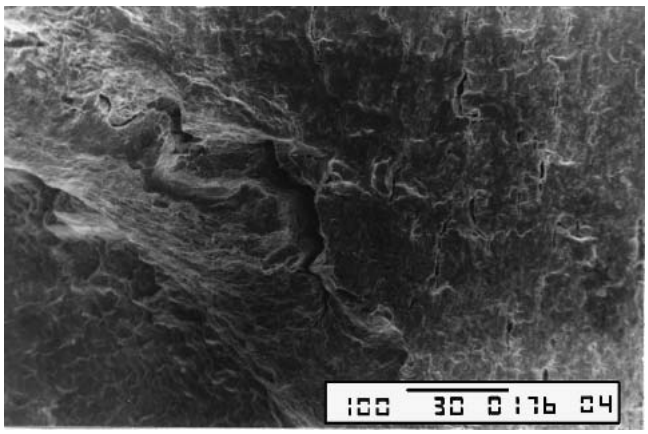

Fig. 16 Tortuous secondary crack in the fracture surface of fatigued tempered steel

dispersions persists for some time before spheroidization sets in at 700 °C. Figure 15 exhibits the fine dispersion of VC precipitates. Outlines of previous martensite plates continue to persist. Compared to VC, Cr_7C_3 coarsens more rapidly (Fig. 9). Molybdenum, however, retards the coarsening of Cr_7C_3, while V tends to stabilize it. Although spherodized structures are known to possess appreciably lower fatigue strength than martensitic structures in unalloyed high-carbon steels,[41] the present work has confirmed the contrary to be true for the microalloy steel. This is attributed primarily to the fine dispersions of VC and Mo_2C, and to a lesser extent to Cr_7C_3 impeding the dislocation glide. Solid solution strengthening of the ferrite by microalloy additions is also expected to have a beneficial effect on fatigue resistance.

Another microstructural change that is observed during tempering is the decomposition of retained austenite to yield thin films of cementite at ferrite grain boundaries. These brittle cementite films reduce the toughness of and provide potential crack nucleation sites along α/Fe_3C interfaces. Smooth, featureless films of Fe_3C are occasionally encountered on fatigue fracture surfaces. Crack path tortuosity such as that illustrated in Fig. 16 suggests that a crack tip deflection mechanism, which probably was provided by the fine dispersions of MACs, could be the prevalent modus operandi for crack propagation in the tempered steel.

4. Conclusions

- The tempered SAE 6150 steel develops the highest tensile strength, fatigue resistance, and endurance limit. These properties are attributed to the presence of fine dispersions of the MACs VC, Mo_2C, and Cr_3O_7, which impede dislocation glide and cause fatigue crack deflection.
- For alternating stress levels above approximately 200 MPa, the fatigue life of the DP steel is about an order of magnitude greater than that of the martensitic variant. While the martensite islets in the DP steel enhance both tensile strength and fatigue resistance by obstructing dislocation movement and crack tip deflection, respectively, the ferrite matrix retards fatigue crack propagation by facilitating crack tip blunting.
- Residual stresses associated with martensite transformation, microcracks inherently present in martensite plates, and strain incompatibility between retained austenite and martensite are thought to be the main factors responsible for the inferior tensile and fatigue properties of the martensitic SAE 6150 steel.

References

1. S. Hayami and F. Frukawa: "Dual Phase and Trip Steels" in *Proceedings of Microalloying '75*, Union Carbide, New York, NY, 1975, pp. 311-21.
2. M.S. Rashid: *SAE Trans.*, *85*, 1976, p. 938.
3. M.S. Rashid, *SAE Trans.*, *86*, 1977, p. 935.
4. J.H. Bucher and E.G. Hamburg: *SAE Trans.*, *86*, 1977, p. 730.
5. A.P. Coldren and G. Tither: *J. Metals*, *30*, 1978, p. 6.
6. G.R. Speich, V.A. Dermarest, and R.L. Miller: *Metall. Trans.*, *12A*, 1981, p. 1419.
7. J.M. Rigsbee and P.J. Vander: in *Formable and Dual Phase Steels*, A.T. Davenport, ed., TMS-AIME, New York, NY, 1979, p. 56.
8. G.R. Eldis: in *Structure and Properties of Dual Phase Steels*, R.A. Kot and J.W. Morris, ed., AIME, New York, NY, 1979, p. 202.
9. T. Furukawa, H. Morikawa, H. Takechi, and K. Koyama: in *Structure and Properties of Dual Phase Steels*, R.A. Kot and J.W. Morris, ed., AIME, New York, NY, 1979, p. 281.
10. R. Priestner and M. Ajmal: *Mater. Sci. Technol.*, *3*, 1987, p. 360.
11. Z. Nishiyama: *Martensitic Transformation*, Academic Press, New York, NY, 1978.
12. M.S. Rashid and B.V.N. Rao: in *Fundamentals of Dual-Phase Steels*, R.A. Kot and B.L. Brambit, ed., TMS-AIME, Warrendale, PA, 1981, p. 249.
13. X.P. Shen and R. Priestner: *Metall. Trans.*, *21A*, 1990, p. 2547.
14. G.M. Hughes: "The Influence of Prior Microstructure on the Constitution of Dual-Phase Steel," M.Sc. Thesis, The University of Manchester, 1986.
15. R. Priestner: in *Proceedings of Phase Transformations '87*, G.M. Lorimer, ed., Institute of Metals, London, UK, 1988, p. 411.
16. S.S. Hansen and B.L. Bramfitt: in *Proceedings of International Conference on Steel Rolling*: *Science and Technology of Flat Rolled Products*, Iron and Steel Institute of Japan, Tokyo, Japan, 1980, p. 1297.
17. T. Kato, K. Hashiguchi, I. Takahashi, T. Irie, and N. Ohashi: in *Fundamentals of Dual-Phase Steels*, R.A. Kot and B.L. Branfitt, ed., TMS-AIME, Warrendale, PA, 1981, p. 199.
18. H. Suzuki and A.J. McEvily: *Metall. Trans.*, *10A*, 1979, p. 475.
19. K. Minakawa, Y. Matsuo, and A.J. McEvily: *Metall. Trans.*, *13A*, 1982, p. 439.
20. V.B. Dutta, S. Suresh, and R.O. Ritchie: *Metall. Trans.*, *15A*, 1984, p. 1193.
21. Jian Ku Shang, J.L. Tzou, and R.O. Ritchie: *Metall. Trans.*, *18A*, 1987, p. 1613.
22. R.M. Ramage, K.V. Jata, G.J. Shiflet, and E.A. Starke, Jr.: *Metall. Trans.*, *18A*, 1987, p. 1291.
23. D.L. Chen, Z.G. Wang, X.X. Jiang, S.H. Ai, and C.H. Shih: *Mater. Sci. Eng.*, *108A*, 1989, p. 141.
24. Y.S. Zheng, Z.G. Wang, and S.H. Ai: in *Proceedings of C-MRS International '90*, *June 18-22, Beijing, People's Republic of China*, Vol. 5, 1990, p. 257.
25. G. Thomas, J.K. Kim D. Manojlovic, and R. Milovic: in *Proceedings of International Symposium on Processing, Microstructrue and Properties of HSLA Steels*, A.J. DeArdo, Jr., ed., TMS, Warrendale, PA, 1988, p. 399.
26. R.W.K. Honeycombe: *Steels, Microstructure and Properties*, Edward Arnold, (Publishers) Ltd., London, UK, 1981.
27. K. Narita: *Trans. Iron Steel Inst. Japan*, *15*, 1975, p. 147.
28. H. Tofaute and E. Buttinghouse: *Archiv. Eisenhuttenwesen*, *12*, 1938, p. 33 (in German).
29. D.P. Koistinen and R.E. Marburger: *Acta Met.*, *7*, 1959, p. 59.

30. A.J. DeArdo, G.A. Rwtz, and P.J. Wray, ed.: *Thermomechanical Processing of Microalloyed Austenite*, TMS-AIME, Warrendale, PA, 1982.
31. G. Krauss: *Principles of Heat Treatment of Steel*, ASM, Metals Park, OH, 1982.
32. G.R. Speich: *Metall. Trans.*, *3A*, 1972, p. 1045.
33. G. Thomas: *Metall. Trans.*, *9A*, 1978, p. 439.
34. A.R. Marder and A.O. Benscoter: *Trans. ASM*, *61*, 1968, p. 239.
35. J.M. Meyer and G.S. Ansell: *Metall. Trans.*, *6A*, 1975, p. 178.
36. D.S. Dabkowski and G.R. Speich: in *Proceedings of Mechanical Working and Steel Processing Conference XV*, AIME, New York, NY, 1977, p. 284.
37. M. Hillert: *Jerkontorets Annaler*, *141*, 1957, p. 67 (in Swedish).
38. Anon.: *Metals Handbook*, Vol 1, 9th ed., ASM, Metals Park, OH, 1978, p. 677.
39. M. Cohen: *Trans. AIME*, *224*, 1962, p. 638.
40. Anon.: *Metals Handbook*, Vol 1, 9th ed., ASM, Metals Park, OH, 1978, p. 676.
41. Howard E. Boyer, ed.: *Atlas of Fatigue Curves*, ASM, Metals Park, OH, 1986, p. 122.